This is the accepted manuscript made available via CHORUS. The article has been published as:

Quantum many-body simulations of the two-dimensional Fermi-Hubbard model in ultracold optical lattices

Bin-Bin Chen, Chuang Chen, Ziyu Chen, Jian Cui, Yueyang Zhai, Andreas Weichselbaum, Jan von Delft, Zi Yang Meng, and Wei Li

Phys. Rev. B **103**, L041107 — Published 19 January 2021

DOI: 10.1103/PhysRevB.103.L041107

Quantum Many-Body Simulations of the 2D Fermi-Hubbard Model in Ultracold Optical Lattices

Bin-Bin Chen,[1,2] Chuang Chen,[3,4] Ziyu Chen,[1] Jian Cui,[1] Yueyang Zhai,[5]
Andreas Weichselbaum,[6,2,*] Jan von Delft,[2] Zi Yang Meng,[7,3,8,†] and Wei Li[1,9,‡]

[1]*School of Physics and Key Laboratory of Micro-Nano Measurement-Manipulation and Physics (Ministry of Education), Beihang University, Beijing 100191, China*
[2]*Arnold Sommerfeld Center for Theoretical Physics, Center for NanoScience, and Munich Center for Quantum Science and Technology, Ludwig-Maximilians-Universität München, 80333 Munich, Germany*
[3]*Beijing National Laboratory for Condensed Matter Physics and Institute of Physics, Chinese Academy of Sciences, Beijing 100190, China*
[4]*School of Physical Sciences, University of Chinese Academy of Sciences, Beijing 100190, China*
[5]*Research Institute of Frontier Science, Beihang University, Beijing 100191, China*
[6]*Department of Condensed Matter Physics and Materials Science, Brookhaven National Laboratory, Upton, New York 11973-5000, USA*
[7]*Department of Physics and HKU-UCAS Joint Institute of Theoretical and Computational Physics, The University of Hong Kong, Pokfulam Road, Hong Kong SAR, China*
[8]*Songshan Lake Materials Laboratory, Dongguan, Guangdong 523808, China*
[9]*International Research Institute of Multidisciplinary Science, Beihang University, Beijing 100191, China*

(Dated: December 8, 2020)

Understanding quantum many-body states of correlated electrons is one main theme in modern condensed matter physics. Given that the Fermi-Hubbard model, the prototype of correlated electrons, has been recently realized in ultracold optical lattices, it is highly desirable to have controlled numerical methodology to provide precise finite-temperature results upon doping, to directly compare with experiments. Here, we demonstrate the exponential tensor renormalization group (XTRG) algorithm [Phys. Rev. X **8**, 031082 (2018)], complemented with independent determinant quantum Monte Carlo (DQMC), offer a powerful combination of tools for this purpose. XTRG provides full and accurate access to the density matrix and thus various spin and charge correlations, down to unprecedented low temperature of few percents of the tunneling energy. We observe excellent agreement with ultracold fermion measurements at both half-filling and finite-doping, including the sign-reversal behavior in spin correlations due to formation of magnetic polarons, and the attractive hole-doublon and repulsive hole-hole pairs that are responsible for the peculiar bunching and antibunching behaviors of the antimoments.

Introduction.— The Fermi-Hubbard model (FHM), describing a paradigmatic quantum many-body system [1, 2], has relevance for a broad scope of correlation phenomena, ranging from high-temperature superconductivity [3], metal-insulator transition [4], quantum criticality [5], to interacting topological states of matter [6]. Yet, puzzles remain in this strongly interacting many-body model after several decades of intensive investigations. In solid-state materials, FHM is often complicated by multi-band structures and interactions such as spin-orbital and Hund's couplings [7]. In this regard, recent progresses in two-dimensional (2D) fermionic optical lattices, where the interplay between the spin and charge degrees of freedom in FHM has been implemented in a faithful way [8–14], enable a very clean and powerful platform for simulating its magnetic [15–22] and transport properties [23, 24].

With the state-of-the-art quantum gas microscope techniques, single-site and spin-resolved imaging is now available, and "snapshots" of correlated fermions have been studied experimentally [8–10, 12]. On top of that, detailed local spin and charge correlations [11, 13–15, 17, 22], as well as hidden orders revealed by pattern recognition [19, 20], all inaccessible in traditional solid-state experiments, can be read out by the microscope. As a highly controlled quantum simulator, ultracold fermions in optical lattices therefore serve as a promising tool for resolving various intriguing theoretical proposals in 2D FHM. However, numerous challenges remain, both theoretically and experimentally. The currently lowest achievable temperature is $T/t \simeq 0.25$-0.5 (with t the fermion tunneling energy) on a finite-size system with about 70-80 ^{6}Li atoms [17, 20, 22], and $T/t \sim 1$ in ^{40}K systems [12, 25]. These temperatures are still much higher than the estimated superconductivity transition temperature, $T_c/t \sim 0.05$, near the optimal doping of the square-lattice FHM [3, 26].

On the theoretical side, it is then of vital importance to provide precise quantum many-body calculations in 2D FHM with similar system size and fermion density as those studied experimentally. With that, one can benchmark theory with experiment, determine the effective temperature of the fermionic optical lattice system, explain experimental results, and provide accurate guidance for future progress. However, accurately computing properties of 2D FHM at finite temperature and finite doping is difficult. Quantum Monte Carlo (QMC) methods suffer from the minus-sign problem, although with finite size and temperature it can actually be performed, yielding unbiased results before one hits the "exponential wall". In this regard, it is highly desirable to have an alternative and powerful method, whose accessible parameter space extends to more difficult yet highly interested regions. In this letter, we demonstrate that the thermal tensor network approach constitutes the method of choice.

In fact, various tensor renormalization group (TRG) meth-

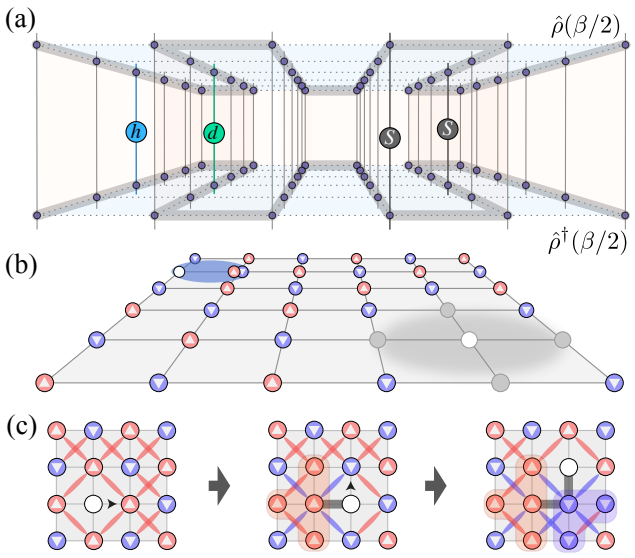

FIG. 1. (a) Bilayer calculation of the spin-spin $\langle \hat{S}_i \cdot \hat{S}_j \rangle$ and hole-doublon $\langle \hat{h}_i \cdot \hat{d}_j \rangle$ correlators by sandwiching corresponding operators in between $\hat{\rho}(\beta/2)$ and $\hat{\rho}^\dagger(\beta/2)$ where the snake-like ordering of sites for the XTRG is indicated by thick gray lines. (b) In the low-temperature AF background (blue down and red up spins), a magnetic polaron (grey shaded region) emerges around a moving hole, where the spins around the hole can be in a superposition of spin-up and down states. The blue ellipse represents a hole-doublon pair showing a strong bunching effect. (c) A hole moves in the system along the path indicated by the grey string, leading to a sign reversal of the diagonal spin correlation. The red- and blue-shaded regions illustrate the deformed magnetic background due to the interplay between the hole and spins. Diagonal correlations are indicated red (aligned) or blue (antialigned).

ods have been developed to compute the ground-state properties of the 2D FHM [27–34]. However, the $T > 0$ properties at finite doping are much less explored. In this work, we generalize the exponential TRG (XTRG) from spin systems [35, 36] to strongly interacting fermions, and employ it to simulate FHM at both half-filling and finite-doping, down to a few percents of the tunneling energy t. We compare the results obtained from both XTRG and determinant QMC (DQMC) [37] in the parameter space where both methods are applicable, and find excellent agreement between them. Then we carry out XTRG+DQMC investigations of the 2D FHM to cover the entire parameter space accessed by current cold-atom experiments. We find that the experimental data can be perfectly explained by our numerical simulations. The combined XTRG+DQMC scheme therefore opens a route for systematic investigation of the finite-temperature phase diagram of the 2D FHM and constitutes an indispensable theoretical guide for ultracold fermion experiments.

The Fermi-Hubbard model.— We consider the interacting electrons on the $L \times L$ square lattice with open boundary condition,

$$H = -t \sum_{\langle i,j\rangle,\sigma} (\hat{c}^\dagger_{i,\sigma}\hat{c}_{j,\sigma} + h.c.) + U \sum_i \hat{n}_{i\uparrow}\hat{n}_{i\downarrow} - \mu \sum_{i,\sigma} \hat{n}_{i,\sigma}, \quad (1)$$

with $t = 1$ the nearest-neighbor hopping amplitude (that sets the unit of energy, throughout), $U > 0$ the on-site Coulomb repulsion, and μ the chemical potential. The fermionic operator $\hat{c}_{i,\sigma}$ annihilates an electron with spin $\sigma \in \{\uparrow, \downarrow\}$ on site i, and $\hat{n}_{i,\sigma} \equiv \hat{c}^\dagger_{i,\sigma}\hat{c}_{i,\sigma}$ is the local number operator.

In the large-U limit ($U \gg t$) and at half-filling ($\mu = U/2$), FHM can be effectively mapped to the Heisenberg model with exchange $J = 4t^2/U$, giving rise to a Néel-ordered ground state with strong antiferromagnetic (AF) correlations at low temperature [depicted schematically in Fig. 1(b)]. This has been demonstrated in many-body calculations [38] and recently observed in ultracold fermion experiments [17]. To make direct comparison to recent experiments [12, 17, 20, 25], we take $L = 4, 6, 8$, set $U = 7.2$ and further tune the chemical potential $\mu < U/2$ to introduce hole doping.

Fermion XTRG.— Finite-temperature TRG methods have been proposed to compute the thermodynamics of interacting spins [35, 39–45]. However, the simulation of correlated fermions at finite temperature has so far been either limited to relatively high temperature [46, 47] or to rather restricted geometries, like 1D chains [48]. XTRG employs a density-matrix renormalization group (DMRG) type setup for both 1D and 2D systems [35, 36] and cools down the systems exponentially fast. It has shown great precision in quantum spin systems [35, 49, 50], thus holding great promise to be generalized to correlated fermions.

As shown in Fig. 1(a), we represent the density matrix $\hat{\rho}(\beta/2)$ as a matrix product operator (MPO) defined on a 1D snake-like path [thick gray lines in Fig. 1(a)]. To guaranteer the positive-definite condition of the density matrix and accurately compute the expectation value of an observable $\hat{O}$, we adopt the bilayer technique [48], yielding $\langle \hat{O} \rangle = \frac{1}{\mathcal{Z}} \mathrm{Tr}[\hat{\rho}(\beta/2) \cdot \hat{O} \cdot \hat{\rho}^\dagger(\beta/2)]$, with $\mathcal{Z} = \mathrm{Tr}[\hat{\rho}(\beta/2) \cdot \hat{\rho}^\dagger(\beta/2)]$ the partition function. We consider mainly two-site static correlators, $\langle \hat{O} \rangle = \langle \hat{O}_i \cdot \hat{O}_j \rangle$, with $\hat{O}_i$ a local operator such as the SU(2) spinor $\hat{S}_i \equiv [\frac{-1}{\sqrt{2}}\hat{c}^\dagger_{i\uparrow}\hat{c}_{i\downarrow}, \frac{1}{2}(\hat{n}_{i\uparrow} - \hat{n}_{i\downarrow}), \frac{1}{\sqrt{2}}\hat{c}^\dagger_{i\downarrow}\hat{c}_{i\uparrow}]^T$, the fermion number $\hat{n}_i \equiv \hat{n}_{i\uparrow} + \hat{n}_{i\downarrow}$, the occupation projectors $\hat{h}_i \equiv |0\rangle\langle 0|_i$ (hole) and $\hat{d}_i \equiv |\uparrow\downarrow\rangle\langle\uparrow\downarrow|_i \equiv \hat{n}_{i\uparrow}\hat{n}_{i\downarrow}$ (doublon), etc. The spin-spin $\langle \hat{S}_i \cdot \hat{S}_j \rangle$ and hole-doublon $\langle \hat{h}_i \cdot \hat{d}_j \rangle$ correlations are schematically depicted in Fig. 1(a).

We also fully implement non-Abelian spin and particle-hole symmetries in the QSpace framework [51, 52] (for technical details, see [71]). To be specific, for the half-filled case we exploit $\mathrm{SU(2)_{charge}} \otimes \mathrm{SU(2)_{spin}}$, and for the doped case $\mathrm{U(1)_{charge}} \otimes \mathrm{SU(2)_{spin}}$ symmetry. The implementation of symmetries has been shown to be very useful in the DMRG-type calculations [53–55], and here it allows us to reduce the D states retained in XTRG to an effective dimension of D^* multiplets. Practically, for the half-filled (doped) cases, the effective dimensional reductions $D/D^* \sim 5.6(2.6)$, corresponding to a $(D/D^*)^4 \simeq$ 50-1000 fold reduction of computation time, guaranteeing high efficiency and accuracy for the thermal simulations. We obtain well-converged XTRG results on the $L = 8$ square lattice at half filling (total site number $N = L^2 = 64$) using up to $D^* = 900$ multiplets ($D \simeq 5,000$

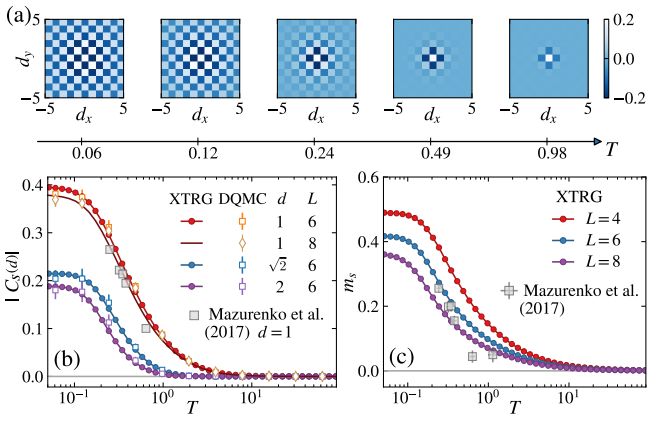

FIG. 2. Half-filled FHM with $U = 7.2$ and $L = 4, 6, 8$. (a) The finite-size AF order pattern is determined from the spin correlation $C_S(d)$ versus (d_x, d_y), which melts gradually as T increases. We show in (b) the spin correlation function $|C_S(d)|$ of various $d = 1, \sqrt{2}, 2$, and in (c) the finite-size spontaneous magnetization m_s. Excellent agreement between the calculated ($L = 8$) data to the experimental data [17] can be observed.

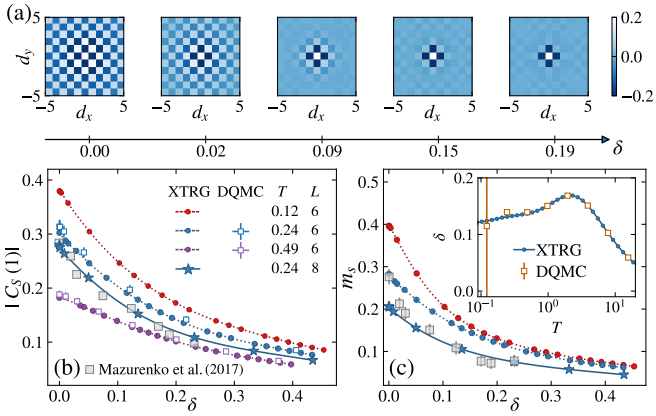

FIG. 3. Doped FHM with $U = 7.2$ and $L = 6, 8$. (a) shows the spin correlation pattern $C_S(d)$ versus δ, plotted at $T = 0.06$, where the finite-size AF order fades out for $\delta \gtrsim 0.15$. The computed (b) spin correlations $|C_S(d = 1)|$ and (c) staggered magnetization m_s are compared to the experimental data [17]. The XTRG data in (b,c) are obtained via extrapolation $1/D^* \to 0$ [71]. In the inset of (c), we show how δ, computed by both XTRG and DQMC, varies with T and on a $L = 6$ lattice and at a fixed chemical potential $\mu = 1.5$.

states), and upon doping using up to $D^* = 1,200$ multiplets ($D \simeq 3,100$ states) [71] down to temperatures $T/t \simeq 0.06$ which is unprecedentedly low for such system sizes. The DQMC simulation performed here is of the finite temperature version with fast update [56].

Spin correlations and finite-size magnetic order at half-filling.— In recent experiments of FHM, the antiferromagnet (AF) has been realized in ultracold optical lattices at low effective temperature $T/t < 0.4$ [17]. We first benchmark the XTRG method, along with DQMC, with the experimental results of half-filled FHM. Fig. 2(a) exhibits the spin correlations $C_S(d) \equiv \frac{1}{N_d}\sum_{|i-j|=d}\frac{\langle \hat{S}_i \cdot \hat{S}_j\rangle}{S(S+1)}$, summed over all N_d pairs of sites i and j (Cartesian coordinates) with distance d. It shows AF magnetic order across the finite-size system at low temperature, e.g., $T \lesssim 0.12$, which melts gradually as temperature increases and effectively disappears above $T \sim 0.49$, in good agreement with recent experiments [17]. In Fig. 2(b), we show $|C_S(d)|$ vs. T at three fixed distances $d = 1, \sqrt{2}, 2$, where XTRG and DQMC curves agree rather well in the whole temperature range. Fig. 2(c) shows the finite-size spontaneous magnetization $m_s \equiv \sqrt{S(\pi, \pi)}$ vs. T, where $S(q) = \frac{1}{N(N-1)}\sum'_{i,j}\frac{\langle \hat{S}_i \cdot \hat{S}_j\rangle}{S(S+1)}e^{-iq\cdot(i-j)}$ is the spin structure factor, with the summation Σ' excludes on-site correlations (following the convention from experiments [17]). For all sizes considered, m_s grows quickly as T is decreased from 1 to 0.1. Notably, for both spin correlations and spontaneous magnetization, the $L = 8$ XTRG data shows good qualitative agreement with the experimental measurements. This may be ascribed to the similar system sizes and boundary conditions [17].

Staggered magnetization upon hole doping.— By tuning the chemical potential $\mu < U/2$, we dope holes into the system and study how they affect the magnetic properties. Fig. 3(a) shows the spin correlation patterns for different dopings δ at low T. The AF order clearly seen at low doping, becomes increasingly short ranged as δ increases, effectively reduced to nearest-neighbor (NN) only for $\delta \gtrsim 0.15$. The fall-off of AF order upon doping can also be observed in $|C_S(d)|$ with a fixed distance d. In Fig. 3(b), we show the $d = 1$ NN spin correlations, where the XTRG and DQMC agree well, whenever the latter is available (for $L = 6$ lattice at $T = 0.24$ and $T = 0.49$). Remarkably, our $L = 8$ XTRG data again show excellent agreement with the experiments, while the sign problem hinders DQMC from reaching such system size at $T = 0.24$ [71].

Fig. 3(c) shows the staggered magnetization m_s vs. δ. Again a rapid drop of the finite-size AF order at approximately $\delta \in [0.1, 0.25]$ can be seen. Based on the agreements between the XTRG ($L = 8$) and experimental results [Fig. 3(b,c)], we find the effective temperature of ultracold fermions in the doped case is also around $T/t = 0.24$, consistent with the experiments [17]. In our calculations we tune the doping δ by scanning the chemical potentials μ. In the inset of Fig. 3(c), we show the doping δ vs. T for a fixed $\mu = 1.5$ (again the XTRG and DQMC results agree for $T \gtrsim 0.24$ with a tolerable sign problem [71] for DQMC). The behavior of δ is non-monotonic: it first increases as T is lowered [having $\delta(T = \infty) = 0$], and then slowly decreases due to hole repulsion [71].

Two-point spin correlations upon hole doping.— In Fig. 4, we analyze spin correlations between the diagonal (d= $\sqrt{2}$) and next-nearest-neighbor (d=2, NNN) sites. We compare them to recent measurements where the diagonal correlation $C_S(\sqrt{2})$ undergoes a sign reversal around $\delta \simeq 0.2$ [20]. Our computations reproduce this fact [Fig. 4(a)], and the $L = 8$ XTRG results computed at $T = 0.24$ accurately reproduce the experimental measurements. For the NNN correlations

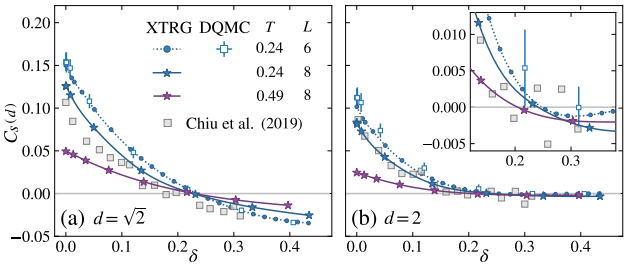

FIG. 4. Diagonal and NNN $C_S(d)$ correlations versus δ for $L \times L$ system with $U = 7.2$ and $L = 6, 8$ for (a) $d = \sqrt{2}$ and (b) $d = 2$. The inset to (b) zooms in on small $C_S(d)$ values. The sign-reversal of C_d is in good agreement with experimental data [20].

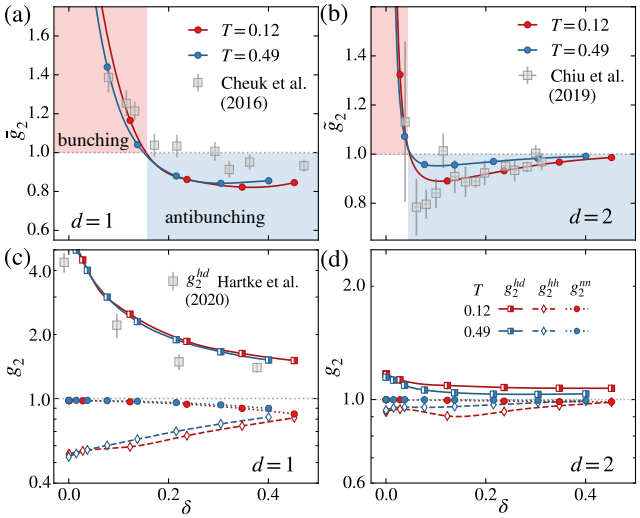

FIG. 5. Various g_2 correlators for a 8×8 system with $U = 7.2$. The antimoment correlators (a) $\bar{g}_2(d = 1)$ and (b) $\tilde{g}_2(d = 2)$ are shown versus δ. Experimental data with $d = 1$, $T/t \simeq 1.0$ [13] and $d = 2$, $T/t \simeq 0.25$ [20] are included for comparison. (c, d) The two-site hole-doublon (g_2^{hd}), hole-hole (g_2^{hh}), and full-density (g_2^{nn}) correlations, for (c) $d = 1$ and (d) $d = 2$. The $d = 1$ hole-doublon correlations g_2^{hd} is compared with experiment in (c), with a nice agreement despite a separate $U/t \simeq 11.8$ in experiment [25].

($d = 2$) [Fig. 4(b)], we find that an analogous sign reversal, hardly discernible in experiments, takes place around $\delta \simeq 0.25$.

The sign reversal can be explained within the geometric string theory [57]. It signals the formation of a magnetic polaron in the system. As shown in Fig. 1(c), the hole motion through the system generates a string of misaligned spins. The strong NN AF spin correlations are thus mixed with the diagonal and even further correlations, e.g., $C_S(2)$, resulting in even ferromagnetic clusters [red and blue shaded regions in Fig. 1(c)]. Due to the interplay between the charge impurity and magnetic background, the moving hole distorts the nearby AF background [see the gray "cloud" in Fig. 1(b)], giving rise to the magnetic polaron. Such exotic quasi-particles have been imaged experimentally [22] for a doublon in the particle-doped Fermi-Hubbard model, and investigated numerically in the context of t-J model [58].

Hole-doublon bunching and hole-hole antibunching.— Quantum gas microscope can also access parity-projected *antimoment* correlation functions defined in the charge sector, $\bar{g}_2(d) \equiv \frac{1}{N_d}\sum_{|i-j|=d}\frac{\langle\hat{\alpha}_i\hat{\alpha}_j\rangle}{\langle\hat{\alpha}_i\rangle\langle\hat{\alpha}_j\rangle}$ [13] and $\tilde{g}_2(d) \equiv \frac{1}{N_d}\sum_{|i-j|=d}[\frac{1}{\delta^2}(\langle\hat{\alpha}_i\hat{\alpha}_j\rangle - \langle\hat{\alpha}_i\rangle\langle\hat{\alpha}_j\rangle)+1]$ [20], with the antimoment projector $\hat{\alpha}_i \equiv \hat{h}_i + \hat{d}_i$ [59]. Fig. 5(a,b) shows the computed antimoment correlation results. Antimoments are bunching ($\bar{g}_2 > 1$) at low doping, yet become antibunching ($\bar{g}_2 < 1$) at large doping, in quantitative agreement with an earlier ^{40}K experiment [13] and a more recent ^{6}Li gas measurement [20]. The antibunching at large doping is attributed to hole repulsion, and the bunching at low-doping to hole-doublon pairs [13].

Now antimoments contain contributions from both, holes and doublons, yet their individual contributions cannot be distinguished via parity projection measurements [13, 20]. XTRG, however, readily yields detailed correlators $g_2^{ll'}(d) \equiv \frac{1}{N_d}\sum_{|\mathbf{i}-\mathbf{j}|=d}\frac{\langle\hat{l}_i\hat{l}'_j\rangle}{\langle\hat{l}_i\rangle\langle\hat{l}'_j\rangle}$, with $l \in \{h, d\}$ and $\hat{l}_i \in \{\hat{h}_i, \hat{d}_i\}$ for hole or double-occupancy projectors, respectively. Later we also use $l = n$ for $\hat{l}_j = \hat{n}_j$ the local density.

Our results for the correlations $g_2^{hh}(d)$ and $g_2^{hd}(d)$ vs. δ are shown in Fig. 5(c,d). We always find anticorrelation amongst holes ($g_2^{hh} < 1$) while strong bunching between hole and doublon ($g_2^{hd} > 1$). As shown in Fig. 5(c), the computed g_2^{hd} data show qualitative agreement with very recent experimental measurements using the full-density-resolved bilayer readout technique [25, 60]. The change from bunching to antibunching behaviors in antimoment correlations in Fig. 5(a,b) can be ascribed to the fact that the hole-doublon attraction is advantageous over the hole-hole repulsion at low doping while the latter dominates at relatively large doping [71]. When comparing the charge correlations at $d = 1$ and 2 in Fig. 5(c,d), we find that the hole-doublon bunching effect in $\bar{g}_2(1)$ is particularly strong at $\delta \ll 1$, where the holes mostly stem from NN hole-doublon pairs [see illustration in Fig. 1(b)]. The further-ranged $g_2^{hd}(2)$ still shows the bunching effect, yet gets much reduced.

The full density correlation $g_2^{nn}(d)$ is shown in Fig. 5(c, d). We observe $g_2^{nn}(d) \approx 1$ at low doping for both $d = 1, 2$, i.e., weak non-local charge correlations near half-filling, and a more pronounced anti-correlation $g_2^{nn}(d) < 1$ as δ increases. Based on our XTRG results, we further reveal that the longer-ranged $g_2^{nn}(2)$ also exhibits anticorrelations upon doping, suggesting the statistical Pauli holes may be rather nonlocal, though decaying rapidly spatially.

Conclusion and outlook.— In this work, we generalized XTRG [35, 36] to the 2D FHM. Employing XTRG and DQMC, we obtained reliable results both for half-filling and doped cases and found consistency with the ultracold atom experiments. XTRG can explore a broader parameter space, especially in the doped case, than DQMC, which is limited by a minus-sign problem. XTRG+DQMC constitutes

a state-of-the-art complimentary numerical setup for probing the phase diagram of FHM, for SU(2) fermions here and generally SU(N) fermions [61], thanks to the implementation of non-Abelian symmetries [51]. Fundamental questions, such as the explanation of the Fermi arcs and the pseudogap phase [62, 63], with their implications for the breaking of Luttinger's theorem [64–67], or the role of topological order [68–70] are open interesting topics to be studied by XTRG+DQMC and optical lattices.

Acknowledgments.— B.-B.C. and C.C. contributed equally to this work. The authors are greatly indebted to Fabian Grusdt and Annabelle Bohrdt for numerous insightful discussions, and to Thomas Hartke and Martin Zwierlein for providing the original experimental data. W.L., J.C., C.C. and Z.Y.M. are supported by National Natural Science Foundation of China (Nos. 11974036, 11834014, 11921004, 11904018) and the Fundamental Research Funds for the Central Universities. Z.Y.M. is also supported by the RGC of Hong Kong SAR China (Grant Nos. 17303019 and 17301420). The German Research Foundation (DFG) supported this research through WE4819/3-1 (B.-B.C.) and Germany's Excellent Strategy – EXC-2111 – 390814868. A.W. was supported by the U.S. Department of Energy, Office of Basic Energy Sciences, under Contract No. DE-SC0012704. We thank the Center for Quantum Simulation Sciences in the Institute of Physics, Chinese Academy of Sciences, the Computational Initiative at the Faculty of Science at the University of Hong Kong, the Tianhe platforms at the National Supercomputer Centers in Tianjin and Guangzhou, and the Leibniz-Rechenzentrum in Munich for their technical support and generous allocation of CPU time.

* weichselbaum@bnl.gov
† zymeng@hku.hk
‡ w.li@buaa.edu.cn

[1] J. Hubbard, "Electron correlations in narrow energy bands," Proceedings of the Royal Society of London. Series A. Mathematical and Physical Sciences **276**, 238–257 (1963).
[2] M. C. Gutzwiller, "Effect of Correlation on the Ferromagnetism of Transition Metals," Phys. Rev. Lett. **10**, 159–162 (1963).
[3] P. A. Lee, N. Nagaosa, and X.-G. Wen, "Doping a mott insulator: Physics of high-temperature superconductivity," Rev. Mod. Phys. **78**, 17–85 (2006).
[4] P. Fazekas, *Lecture Notes on Electron Correlation and Magnetism*, Series In Modern Condensed Matter Physics (World Scientific Publishing Company, 1999).
[5] S. Sachdev, *Quantum Phase Transitions* (Cambridge University Press, 2011).
[6] X.G. Wen, *Quantum Field Theory of Many-Body Systems: From the Origin of Sound to an Origin of Light and Electrons*, Oxford Graduate Texts (OUP Oxford, 2004).
[7] A. Georges, L. de' Medici, and J. Mravlje, "Strong correlations from Hund's coupling," Annual Review of Condensed Matter Physics **4**, 137–178 (2013).
[8] W. S. Bakr, J. I. Gillen, A. Peng, S. Fölling, and M. Greiner, "A quantum gas microscope for detecting single atoms in a Hubbard-regime optical lattice," Nature **462**, 74–77 (2009).
[9] M. F. Parsons, F. Huber, A. Mazurenko, C. S. Chiu, W. Setiawan, K. Wooley-Brown, S. Blatt, and M. Greiner, "Site-resolved imaging of fermionic ^{6}Li in an optical lattice," Phys. Rev. Lett. **114**, 213002 (2015).
[10] D. Greif, M. F. Parsons, A. Mazurenko, C. S. Chiu, S. Blatt, F. Huber, G. Ji, and M. Greiner, "Site-resolved imaging of a fermionic Mott insulator," Science **351**, 953–957 (2016).
[11] M. Boll, T. A. Hilker, G. Salomon, A. Omran, J. Nespolo, L. Pollet, I. Bloch, and C. Gross, "Spin- and density-resolved microscopy of antiferromagnetic correlations in Fermi-Hubbard chains," Science **353**, 1257–1260 (2016).
[12] L. W. Cheuk, M. A. Nichols, K. R. Lawrence, M. Okan, H. Zhang, and M. W. Zwierlein, "Observation of 2D fermionic Mott insulators of ^{40}K with single-site resolution," Phys. Rev. Lett. **116**, 235301 (2016).
[13] L. W. Cheuk, M. A. Nichols, K. R. Lawrence, M. Okan, H. Zhang, E. Khatami, N. Trivedi, T. Paiva, M. Rigol, and M. W. Zwierlein, "Observation of spatial charge and spin correlations in the 2D Fermi-Hubbard model," Science **353**, 1260–1264 (2016).
[14] M. F. Parsons, A. Mazurenko, C. S. Chiu, G. Ji, D. Greif, and M. Greiner, "Site-resolved measurement of the spin-correlation function in the Fermi-Hubbard model," Science **353**, 1253–1256 (2016).
[15] D. Greif, T. Uehlinger, G. Jotzu, L. Tarruell, and T. Esslinger, "Short-Range Quantum Magnetism of Ultracold Fermions in an Optical Lattice," Science **340**, 1307–1310 (2013).
[16] R. A. Hart, P. M. Duarte, T.-L. Yang, X. Liu, T. Paiva, E. Khatami, R. T. Scalettar, N. Trivedi, D. A. Huse, and R. G. Hulet, "Observation of antiferromagnetic correlations in the hubbard model with ultracold atoms," Nature **519**, 211–214 (2015).
[17] A. Mazurenko, C. S. Chiu, G. Ji, M. F. Parsons, M. Kanász-Nagy, R. Schmidt, F. Grusdt, E. Demler, D. Greif, and M. Greiner, "A cold-atom Fermi–Hubbard antiferromagnet," Nature **545**, 462–466 (2017).
[18] P. T. Brown, D. Mitra, E. Guardado-Sanchez, P. Schauß, S. S. Kondov, E. Khatami, T. Paiva, N. Trivedi, D. A. Huse, and W. S. Bakr, "Spin-imbalance in a 2D Fermi-Hubbard system," Science **357**, 1385–1388 (2017).
[19] T. A. Hilker, G. Salomon, F. Grusdt, A. Omran, M. Boll, E. Demler, I. Bloch, and C. Gross, "Revealing hidden antiferromagnetic correlations in doped Hubbard chains via string correlators," Science **357**, 484–487 (2017).
[20] C. S. Chiu, G. Ji, A. Bohrdt, M. Xu, M. Knap, E. Demler, F. Grusdt, M. Greiner, and D. Greif, "String patterns in the doped Hubbard model," Science **365**, 251–256 (2019).
[21] G. Salomon, J. Koepsell, J. Vijayan, T. A. Hilker, J. Nespolo, L. Pollet, I. Bloch, and C. Gross, "Direct observation of incommensurate magnetism in Hubbard chains," Nature **565**, 56–60 (2019).
[22] J. Koepsell, J. Vijayan, P. Sompet, F. Grusdt, T. A. Hilker, E. Demler, G. Salomon, I. Bloch, and C. Gross, "Imaging magnetic polarons in the doped Fermi–Hubbard model," Nature **572**, 358–362 (2019).
[23] M. A. Nichols, L. W. Cheuk, M. Okan, T. R. Hartke, E. Mendez, T. Senthil, E. Khatami, H. Zhang, and M. W. Zwierlein, "Spin transport in a Mott insulator of ultracold fermions," Science **363**, 383–387 (2019).
[24] P. T. Brown, D. Mitra, E. Guardado-Sanchez, R. Nourafkan, A. Reymbaut, C.-D. Hébert, S. Bergeron, A.-M. S. Tremblay, J. Kokalj, D. A. Huse, P. Schauß, and W. S. Bakr, "Bad metallic transport in a cold atom Fermi-Hubbard system," Science **363**,

379–382 (2019).
[25] T. Hartke, B. Oreg, N. Jia, and M. Zwierlein, "Measuring total density correlations in a Fermi-Hubbard gas via bilayer microscopy," arXiv e-prints (2020), arXiv:2003.11669.
[26] K.-S. Chen, Z. Y. Meng, S.-X. Yang, T. Pruschke, J. Moreno, and M. Jarrell, "Evolution of the superconductivity dome in the two-dimensional hubbard model," Phys. Rev. B **88**, 245110 (2013).
[27] R. M. Noack, S. R. White, and D. J. Scalapino, "The Density Matrix Renormalization Group for Fermion Systems," arXiv e-prints (1994), arXiv:cond-mat/9404100.
[28] P. Corboz, R. Orús, B. Bauer, and G. Vidal, "Simulation of strongly correlated fermions in two spatial dimensions with fermionic projected entangled-pair states," Phys. Rev. B **81**, 165104 (2010).
[29] C. V. Kraus, N. Schuch, F. Verstraete, and J. I. Cirac, "Fermionic projected entangled pair states," Phys. Rev. A **81**, 052338 (2010).
[30] Z.-C. Gu, F. Verstraete, and X.-G. Wen, "Grassmann tensor network states and its renormalization for strongly correlated fermionic and bosonic states," arXiv e-prints (2010), arXiv:1004.2563.
[31] J. P. F. LeBlanc, A. E. Antipov, F. Becca, I. W. Bulik, G. K.-L. Chan, C.-M. Chung, Y. Deng, M. Ferrero, T. M. Henderson, C. A. Jiménez-Hoyos, E. Kozik, X.-W. Liu, A. J. Millis, N. V. Prokof'ev, M. Qin, G. E. Scuseria, H. Shi, B. V. Svistunov, L. F. Tocchio, I. S. Tupitsyn, S. R. White, S. Zhang, B.-X. Zheng, Z. Zhu, and E. Gull (Simons Collaboration on the Many-Electron Problem), "Solutions of the two-dimensional hubbard model: Benchmarks and results from a wide range of numerical algorithms," Phys. Rev. X **5**, 041041 (2015).
[32] B.-X. Zheng, C.-M. Chung, P. Corboz, G. Ehlers, M.-P. Qin, R. M. Noack, H. Shi, S. R. White, S. Zhang, and G. K.-L. Chan, "Stripe order in the underdoped region of the two-dimensional Hubbard model," Science **358**, 1155–1160 (2017).
[33] M. Qin, C.-M. Chung, H. Shi, E. Vitali, C. Hubig, U. Schollwöck, S. R. White, and S. Zhang, "Absence of superconductivity in the pure two-dimensional Hubbard model," arXiv e-prints , arXiv:1910.08931 (2019), arXiv:1910.08931.
[34] C.-M. Chung, M. Qin, S. Zhang, U. Schollwöck, and S. R. White, "Plaquette versus ordinary d-wave pairing in the t'-Hubbard model on a width 4 cylinder," arXiv e-prints , arXiv:2004.03001 (2020), arXiv:2004.03001.
[35] B.-B. Chen, L. Chen, Z. Chen, W. Li, and A. Weichselbaum, "Exponential Thermal Tensor Network Approach for Quantum Lattice Models," Phys. Rev. X **8**, 031082 (2018).
[36] H. Li, B.-B. Chen, Z. Chen, J. von Delft, A. Weichselbaum, and W. Li, "Thermal tensor renormalization group simulations of square-lattice quantum spin models," Phys. Rev. B **100**, 045110 (2019).
[37] X.-J. Han, C. Chen, J. Chen, H.-D. Xie, R.-Z. Huang, H.-J. Liao, B. Normand, Z. Y. Meng, and T. Xiang, "Finite-temperature charge dynamics and the melting of the Mott insulator," Phys. Rev. B **99**, 245150 (2019).
[38] C. N. Varney, C.-R. Lee, Z. J. Bai, S. Chiesa, M. Jarrell, and R. T. Scalettar, "Quantum Monte Carlo study of the two-dimensional fermion Hubbard model," Phys. Rev. B **80**, 075116 (2009).
[39] F. Verstraete, J. J. García-Ripoll, and J. I. Cirac, "Matrix product density operators: Simulation of finite-temperature and dissipative systems," Phys. Rev. Lett. **93**, 207204 (2004).
[40] M. Zwolak and G. Vidal, "Mixed-state dynamics in one-dimensional quantum lattice systems: A time-dependent superoperator renormalization algorithm," Phys. Rev. Lett. **93**, 207205 (2004).
[41] A. E. Feiguin and S. R. White, "Finite-temperature density matrix renormalization using an enlarged hilbert space," Phys. Rev. B **72**, 220401(R) (2005).
[42] W. Li, S.-J. Ran, S.-S. Gong, Y. Zhao, B. Xi, F. Ye, and G. Su, "Linearized tensor renormalization group algorithm for the calculation of thermodynamic properties of quantum lattice models," Phys. Rev. Lett. **106**, 127202 (2011).
[43] B.-B. Chen, Y.-J. Liu, Z. Chen, and W. Li, "Series-expansion thermal tensor network approach for quantum lattice models," Phys. Rev. B **95**, 161104(R) (2017).
[44] B. Bruognolo, Z. Zhu, S. R. White, and E. Miles Stoudenmire, "Matrix product state techniques for two-dimensional systems at finite temperature," arXiv e-prints , arXiv:1705.05578 (2017), arXiv:1705.05578.
[45] C.-M. Chung and U. Schollwöck, "Minimally entangled typical thermal states with auxiliary matrix-product-state bases," arXiv e-prints , arXiv:1910.03329 (2019), 1910.03329.
[46] E. Khatami and M. Rigol, "Thermodynamics of strongly interacting fermions in two-dimensional optical lattices," Phys. Rev. A **84**, 053611 (2011).
[47] P. Czarnik and J. Dziarmaga, "Fermionic projected entangled pair states at finite temperature," Phys. Rev. B **90**, 035144 (2014).
[48] Y.-L. Dong, L. Chen, Y.-J. Liu, and W. Li, "Bilayer linearized tensor renormalization group approach for thermal tensor networks," Phys. Rev. B **95**, 144428 (2017).
[49] L. Chen, D.-W. Qu, H. Li, B.-B. Chen, S.-S. Gong, J. von Delft, A. Weichselbaum, and W. Li, "Two-temperature scales in the triangular-lattice heisenberg antiferromagnet," Phys. Rev. B **99**, 140404(R) (2019).
[50] H. Li, Y. D. Liao, B.-B. Chen, X.-T. Zeng, X.-L. Sheng, Y. Qi, Z. Y. Meng, and W. Li, "Kosterlitz-Thouless melting of magnetic order in the triangular quantum Ising material $TmMgGaO_4$," Nat. Commun. **11**, 1111 (2020).
[51] A. Weichselbaum, "Non-Abelian symmetries in tensor networks : A quantum symmetry space approach," Ann. Phys. **327**, 2972–3047 (2012).
[52] A. Weichselbaum, "X-symbols for non-abelian symmetries in tensor networks," Phys. Rev. Research **2**, 023385 (2020).
[53] I. P. McCulloch and M. Gulácsi, "The non-Abelian density matrix renormalization group algorithm," EPL **57**, 852 (2002).
[54] M. A. Werner, C. P. Moca, Örs Legeza, M. Kormos, and G. Zaránd, "Spin fluctuations after quantum quenches in the S=1 Haldane chain: Numerical validation of the semi-semiclassical theory," Phys. Rev. B **100**, 035401 (2019).
[55] M. A. Werner, C. P. Moca, Örs Legeza, and G. Zaránd, "Quantum quench and charge oscillations in the SU(3) Hubbard model: A test of time evolving block decimation with general non-Abelian symmetries," Phys. Rev. B **102**, 155108 (2020).
[56] F. F. Assaad and H. G. Evertz, "World-line and determinantal quantum Monte Carlo methods for spins, phonons and electrons," in *Computational Many-Particle Physics*, edited by H. Fehske, R. Schneider, and A. Weiße (Springer Berlin Heidelberg, Berlin, Heidelberg, 2008) pp. 277–356.
[57] F. Grusdt, M. Kánasz-Nagy, A. Bohrdt, C. S. Chiu, G. Ji, M. Greiner, D. Greif, and E. Demler, "Parton Theory of Magnetic Polarons: Mesonic Resonances and Signatures in Dynamics," Phys. Rev. X **8**, 011046 (2018).
[58] E. Blomquist and J. Carlström, "Unbiased description of magnetic polarons in a Mott insulator," Commun Phys **3**, 1–5 (2020).
[59] A local (spin) moment is present only at filling $n = 1$. An analogous moment can be defined in the SU(2) particle/hole sector,

which is complimentary to the spin space as it operates within empty and double occupied state, hence 'antimoment'.

[60] J. Koepsell, S. Hirthe, D. Bourgund, P. Sompet, J. Vijayan, G. Salomon, C. Gross, and I. Bloch, "Robust bilayer charge pumping for spin- and density-resolved quantum gas microscopy," Phys. Rev. Lett. **125**, 010403 (2020).

[61] H. Ozawa, S. Taie, Y. Takasu, and Y. Takahashi, "Antiferromagnetic spin correlation of SU($\mathcal{N}$) fermi gas in an optical superlattice," Phys. Rev. Lett. **121**, 225303 (2018).

[62] M. R. Norman, H. Ding, M. Randeria, J. C. Campuzano, T. Yokoya, T. Takeuchi, T. Takahashi, T. Mochiku, K. Kadowaki, P. Guptasarma, and D. G. Hinks, "Destruction of the fermi surface in underdoped high-Tc superconductors," Nature **392**, 157–160 (1998).

[63] B. Keimer, S. A. Kivelson, M. R. Norman, S. Uchida, and J. Zaanen, "From quantum matter to high-temperature superconductivity in copper oxides," Nature **518**, 179–186 (2015).

[64] J. M. Luttinger, "Fermi surface and some simple equilibrium properties of a system of interacting fermions," Phys. Rev. **119**, 1153–1163 (1960).

[65] M. Oshikawa, "Topological approach to luttinger's theorem and the fermi surface of a kondo lattice," Phys. Rev. Lett. **84**, 3370–3373 (2000).

[66] A. Paramekanti and A. Vishwanath, "Extending luttinger's theorem to Z_2 fractionalized phases of matter," Phys. Rev. B **70**, 245118 (2004).

[67] T. Senthil, S. Sachdev, and M. Vojta, "Fractionalized fermi liquids," Phys. Rev. Lett. **90**, 216403 (2003).

[68] S. Gazit, Fakher F. Assaad, and S. Sachdev, "Fermi-surface reconstruction without symmetry breaking," arXiv e-prints , arXiv:1906.11250 (2019), arXiv:1906.11250.

[69] C. Chen, X. Y. Xu, Y. Qi, and Z. Y. Meng, "Metal to orthogonal metal transition," Chin. Phys. Lett. **37**, 047103 (2020).

[70] C. Chen, T. Yuan, Y. Qi, and Z. Y. Meng, "Doped Orthogonal Metals Become Fermi Arcs," arXiv e-prints , arXiv:2007.05543 (2020), arXiv:2007.05543 [cond-mat.str-el] .

[71] In Supplementary Materials, we briefly recapitulate the basic idea of XTRG and its generalization to interacting fermions. The implementation of non-Abelian symmetries is provided in Sec. A. Detailed convergence check and the linear extrapolation $1/D^* \to 0$ for the spin correlation are shown in Sec. B. Complementary XTRG data on the spin and charge correlations in the doped FHM are presented in Sec. C, and Sec. D is devoted to details of DQMC algorithms and calculations.